

On the Interplay of Regional Mobility, Social Connectedness, and the Spread of COVID-19 in Germany

Cornelius Fritz and Göran Kauerman
Department of Statistics, LMU Munich

October 27, 2021

Abstract

Since the primary mode of respiratory virus transmission is person-to-person interaction, we are required to reconsider physical interaction patterns to mitigate the number of people infected with COVID-19. While non-pharmaceutical interventions (NPI) had an evident impact on national mobility patterns, only the relative regional mobility behaviour enables an unbiased perspective on the effect of human movement on the spread of COVID-19. In this paper we therefore investigate the impact of human mobility and social connectivity derived from Facebook activities on the weekly rate of new infections in Germany between March 3rd and June 22nd, 2020. Our results confirm that reduced social activity lowers the infection rate, accounting for regional and temporal patterns. The extent of social distancing, quantified by the percentage of people staying put within a federal administrative district, has an overall negative effect on the incidence of infections. Additionally, our results show spatial infection patterns based on geographic as well as social distances.

Keywords – COVID-19, Infectious Disease Modelling, Semiparametric Regression, Spatial Network Data, Social Connectedness, Social Networks

1 Introduction

The COVID-19 virus outbreak originating in mainland China (Wu et al., 2020) leapt over to Europe and quickly evolved to a global pandemic in March 2020 (WHO, 2020). Only through strict non-pharmaceutical interventions (NPI), most national health systems were able to react to this new threat rapidly. In numerous scientific efforts, physical distancing measures were discovered to be the most effective interventions (Prem et al., 2020; Flaxman et al., 2020) and found to be necessary maybe until 2022 (Kissler et al., 2020). The effectiveness of such measures emanates from researchers confirming that the main form of virus transmission is person-to-person interaction (Chan et al., 2020). In particular, the virus can be spread by inhaling microscopic aerosol particles that contain COVID-19 and remain viable in the air with a half-life of about 1 hour (Van Doremalen et al., 2020; Asadi et al., 2020) or direct contact through the exchange of virus-containing droplets with infected individuals (Guan et al., 2020; Li et al., 2020). Since also, a high percentage of cases are asymptomatic (Lavezzo et al., 2020) or get infected by asymptomatic cases (Li et al., 2020), human mobility can explain the spread of COVID-19 to a large extent (Kraemer et al., 2020).

Stemming from the consequential need to account for contact patterns when modelling the spread of COVID-19, Oliver et al. (2020) list multiple possibilities how, in particular, mobile phone data can help in that regard. To enable this type of analysis, Facebook extended the *Data for Good* program to a broader audience of researchers and provided so-called *Disease Prevention Maps* for multiple countries (Maas et al., 2019). This database includes measurements on quantities like co-location, Facebook population, and movement range derived from information of more than 26 million Facebook users. These data are available on a regional level. Additionally, a measure for the social connectedness between geographic regions is supplied (Bailey et al., 2018). In various studies, the data were employed to demonstrate how the impact of lock-down measures in Italy was more severe for municipalities with higher fiscal capacities (Bonaccorsi et al., 2020), quantify social and geographic spillover effects from relaxations of shelter-in-place orders (Holtz et al., 2020), and predict the number of infections on a fine spatiotemporal resolution using contact tracing data (Lorch et al., 2020).

In this article, we use the Facebook data to analyse how regional differences in mobility patterns and friendship proximity affect the spread of COVID-19 in Germany. While NPIs, e.g., the nationwide shutdown in Germany that started March 22nd, had an evident impact on the nationwide human mobility and ceased the exponential spread of the virus (Flaxman et al., 2020), the effect of the relative movement between regional districts was not yet fully assessed. So far studies concerning human movements during the current pandemic are largely focused on how the lock-down affected national human mobility (Galeazzi et al., 2020) or specific regions regarding their economical status (Bonaccorsi et al., 2020). To fill this gap, we derive covariates from the mobility data to quantify the overall dispersion of meeting patterns and the abidance to social distancing. Through weekly standardisation of the covariates we control for the dynamics therein, which are, in turn, driven by NPIs. Therefore, our research enables a quantitative assessment of different mobility strategies relative to the national average. In addition, we infer positions of the federal administrative regions in a social space from the information on the relative friendship links among them (Bailey et al., 2018) using multidimensional scaling (Cox and Cox, 2000; Borg et al., 2013). Subsequently, we relate the processed data to the weekly rate of COVID-19 infections in Germany between March 3rd and June 22nd, 2020. This

time frame permits the analysis of the dynamic spread starting with the WHO declaring COVID-19 a pandemic (WHO, 2020).

We employ a spatio-temporal regression model for the ratio of local COVID-19 infections that takes autoregressive structures, age and sex-specific effects, contagion by nearby districts in the geographic and social space, as well as latent heterogeneities between the districts into account. Our method is closely related to the surveillance model introduced by Held et al. (2005). They extend generalised linear models to analyse surveillance data from epidemic outbreaks. This approach was expanded to handle multivariate surveillance data (Paul et al., 2008), control for seasonality and spatial heterogeneity (Held and Paul, 2012), and include neighbourhood information from social contact data (Meyer and Held, 2017). Contrasting this type of model, the objective of our model is to illuminate the connection between mobility patterns, social connectivity, and the spread of COVID-19 in an interpretable manner. While forecasting infections is certainly a central objective in epidemic surveillance, this is not the main focus of our work (see also Held et al., 2017).

The rest of the article will be structured as follows: We discuss the data sources, its measures on social interaction as well as mobility and propose an imputation model for missing onset dates in Section 2. In Section 3, we propose a semiparametric spatio-temporal model for the ratio of local COVID-19 infections. The results of the analysis are presented in Section 4. Lastly, Section 5 concludes the article.

2 Data Description

2.1 Data on Social Activity during COVID-19

For Germany, the data are generated from approximately 10 million Facebook users, who enabled geolocation features accessible by Facebook on their devices. To abide by the privacy policies, the observations are anonymised through aggregation onto tile Bing polygons (Microsoft, Microsoft), censoring if not enough users were observed in the spatial region, as well as randomisation using additional noise and spatial smoothing (Maas et al., 2019). Considering that the aim is to draw conclusions on the regional level, we accumulate the polygons to the 401 federal administrative districts in Germany (we set $n = 401$ and a complete list is given by the German Federal Statistical Office). We propose the following measures describing social interaction and mobility. All measures are taken on a weekly level, where simple averaging is used for quantities that are available at a finer temporal resolution.

Co-location: Co-location in week t is measured by the probability $p_{ij,t}$ of a random person from district i to be located in the same $0.6km \times 0.6km$ square as another random person from district j . These probabilities are then used to construct a district-wise quantity for the concentration of meeting patterns using the Gini index, which is given by:

$$x_{i,t,gini} = \frac{\sum_{m,n \neq i} |p_{im,t} - p_{in,t}|}{2n \sum_{j \neq i} p_{ij,t}}$$

If we were to observe the maximal value of 1 in $x_{i,t,gini}$, all people within federal district i would only meet people (i.e. Facebook users) from only one further district. This behaviour is exemplary of an extremely restricted mobility. Conversely, a lower value heuristically indicates dispersed meeting patterns. The temporal paths of the Gini indices for the 401 districts in Germany are depicted in Figure 1 (a). Overall, we note that as the

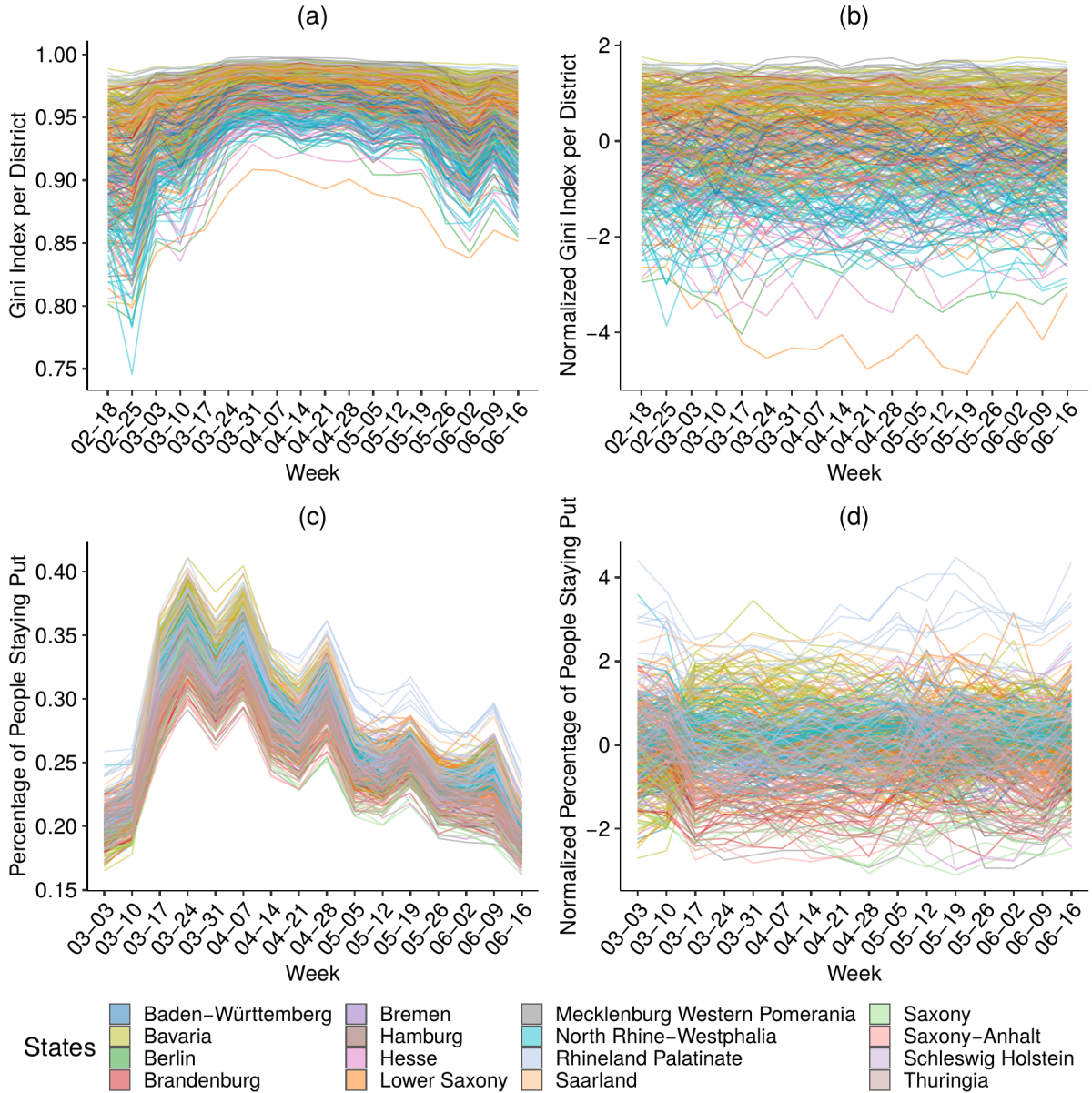


Figure 1: (a): Gini indices for each district over time. (b): Normalised Gini indices for each district over time. (c): Percentages of people staying put for each district over time. (d): Normalised percentages of the people staying put. The colour of the lines indicate the state in which each state is located and the dates (mm:dd) are the first day of the corresponding week.

crisis evolves, the meeting patterns become more concentrated on a few other districts. This behaviour contrasts rather dispersed practices before the pandemic. An upward trend is visible until the nationwide lock-down on 22nd of March, 2020¹. Thereupon, meeting patterns continue to be overall condensed, although the indices slowly decline. To enable a meaningful comparison between the respective estimates in the regression setting of Section 3, we standardise the Gini indices per week, as can be seen in Figure 1 (b).

Percentage Staying Put: Besides the relative attribution of co-location probabilities

¹In Bavaria the lock-down started already on the 16th of March, 2020.

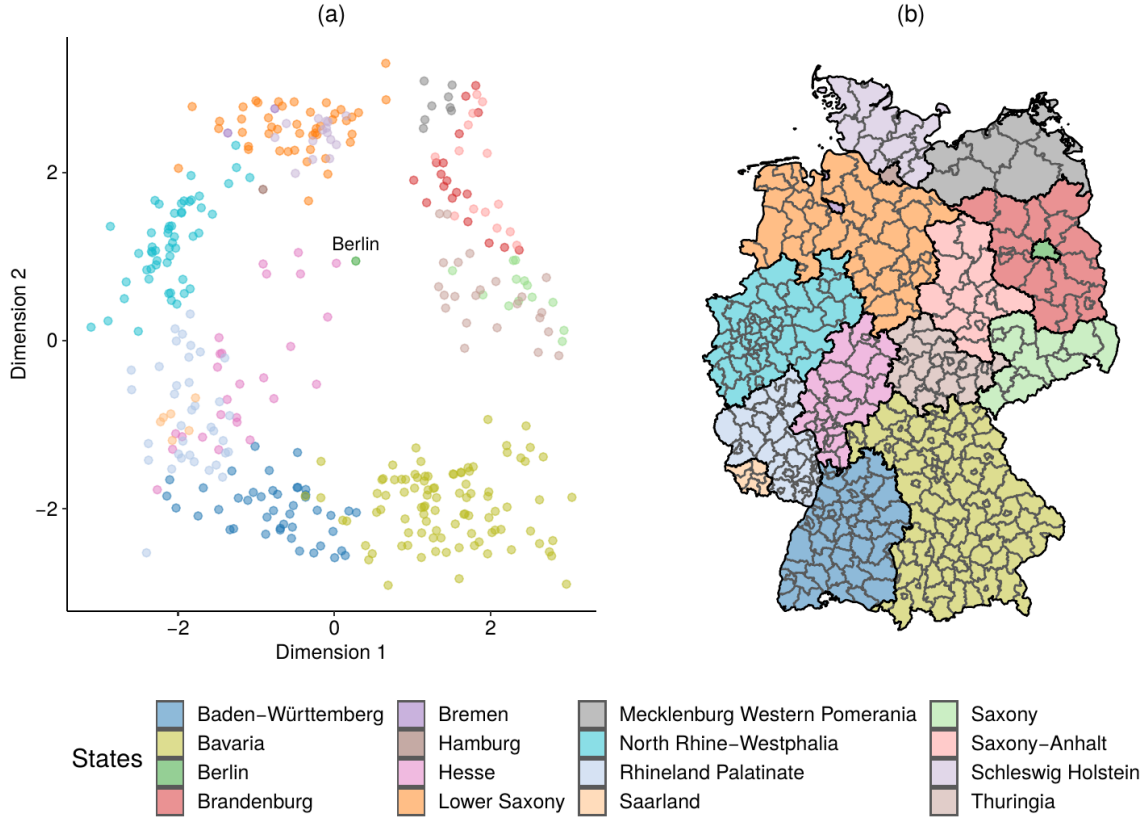


Figure 2: (a): Coordinates representing the friendship distances. The colour of the points indicate the state in which each state is located. (b): Map representing the colour legend.

to other districts, we investigate a measure that expresses how people (Facebook users) comply with social distancing. We quantify this concept by the covariate $x_{i,t,sp}$, which is defined as the average percentage of people in district i staying put during week t . Respective data were collected using geolocation traces of mobile devices and users are defined to be staying put, if they are only observed in one $0.6km \times 0.6km$ square throughout a day (Facebook, Facebook). In Figure 1 (c) clear break-points are visible, giving evidence of the temporary lock-down that started between the 17th and 24th of March. During the following weeks, the observed values gradually level off around pre-lock-down values.

Similarly to the treatment of the Gini index, we standardise the percentages in the regression setting as well. While the visual impression from 1 (c) insinuates that the dynamics of people staying put are similar between districts, the standardised paths, given in Figure 1 (d), reveal local differences between them. For instance, the early look-down in Bavaria resulted in a substantial relative increase of the respective districts between the 10th and 17th of March, see the yellow-green lines.

Friendship Distance: Spatial distance is found to be strongly associated with the spread between regions (Kang et al., 2020). Beyond the geographic proximity, Cho et al. (2011) argued that friendship ties explain specifically long-distance mobility. This type of travel is fundamental for understanding the early spread of the pandemic (Chinazzi et al., 2020). To accommodate this possible line of infection, we include a measure for the strength of friendship ties between the districts of Germany. More precisely, we employ the social connectedness index proposed by Bailey et al. (2018), which is based on an anonymised snapshot of all active Facebook users and their friendship networks from

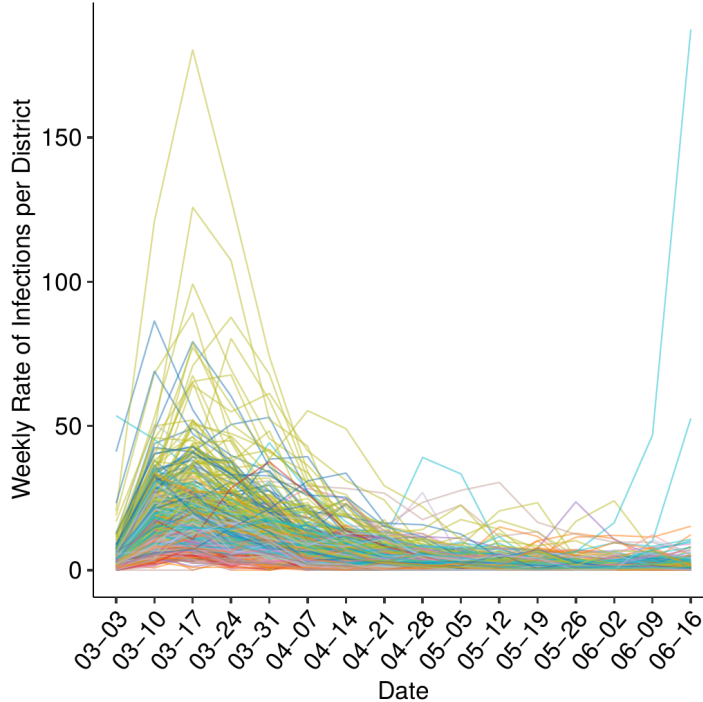


Figure 3: Observed Rate of Weekly Infections for each federal district. The colour of the lines indicate the state in which each state is located, a legend can be found in Figure 2.

April 2020. For the administrative district i and j the time-invariant measure $x_{ij,soc}$ is given by:

$$x_{ij,soc} = \frac{\#\{\text{Friendship Ties between users in district } i \text{ and } j\}}{\#\{\text{Users in district } i\}\#\{\text{Users in district } j\}} \quad \forall i, j \in \{1, \dots, n\}.$$

In a note, Kuchler et al. (2020) uncover high correlations between the social connectedness indices and the spread of COVID-19. This index is further processed to provide a spatial allocation based on social instead of Euclidean distances. To do so, we first transform social connectedness to social distance d_{soc} by taking the reciprocal of connectedness, i.e., $d_{ij,soc} = \frac{1}{x_{ij,soc}}$. Consecutively, we convert these distances to coordinates using multidimensional scaling (Borg et al., 2013). Using standard methods, such as Procrustes analysis, we map the rotation of the inferred coordinates in the friendship space to be most similar to the geographic coordinates (Cox and Cox, 2008). The outcome of the algorithm for each district i is denoted by $x_{i,soc}$ and gives the geo-coordinates in the friendship space as shown in Figure 2. Robust connectivity within federal states and neighbouring districts are visible in the friendship coordinates. We also observe that the capital, Berlin, is situated in the very centre, reflecting its unique and highly connected position. Additionally, one can detect a persisting corridor between districts located in former East- and West-Germany. Technical details on the procedure are given in Annex A.1. Next to the social coordinates we incorporated the geographic coordinates of each district $x_{i,coord}$, i.e., the longitude and latitude of each districts centroid, in our application.

Population Size: We compiled district-, age- and sex-specific population data from the German Federal Statistical Office and denote it by $x_{i,g,pop}$.

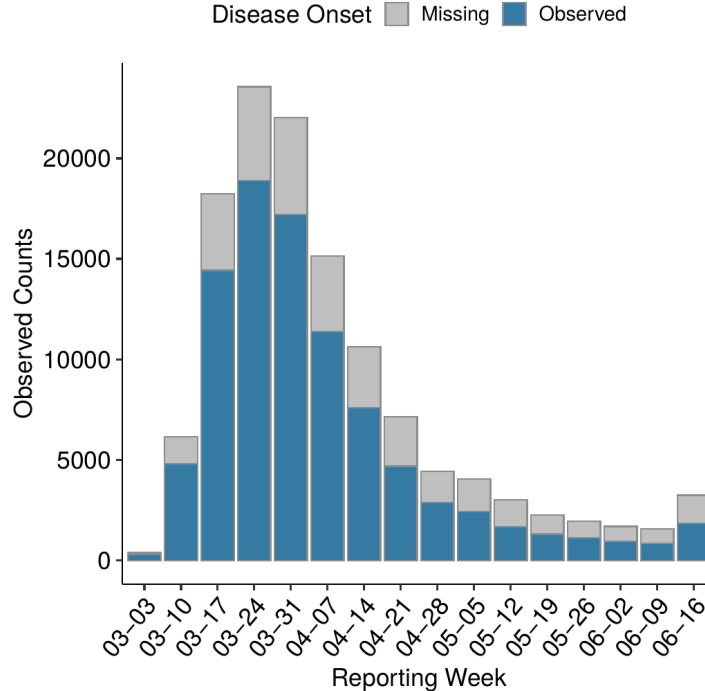


Figure 4: Count of missing and observed disease onset dates per reporting week.

2.2 Data on Infections

The Robert-Koch-Institute provides timely data on the daily number of COVID-19 infections in Germany. We limit the present analysis to individuals, that are between 15 and 59 years old, due to the age structure in the Facebook population. Besides, the given surveillance counts are stratified by age group (15-35 and 36-59) and gender. For each entry, dates of symptom onset and reporting are given, although the onset date is partially missing. Our principal analysis is based on the disease onset date since it ensures more valid information on the infection incidence. Imputation of the missing values is required and we present our method subsequently. By $y_{i,g,t}$ we denote the observed (and partially imputed) counts of new onsets within district i , age/gender-group g and week t . For completeness, we define with $x_{i,g}$ the matching indicator for the age/gender group.

The observed rates are visualised in Figure 3 colour-coded according to the different states. Two districts, namely Guetersloh and Warendorf (North Rhine-Westphalia), experience a local outbreak in the last weeks of the observational period (Kottasová, 2020). Once the first peak of infections could be overcome, the cases in the aftermath are increasingly attributed to these local outbreaks. For example, the local outbreak in North Rhine-Westphalia encompasses 48% of new infections with disease onset in the week starting on the 16th of June.

2.3 Imputation of Disease Onset

In Figure 4 the proportions of missing disease onset per reporting weeks are given. Since approximately 30 % of the onset dates are missing, a complete-case analysis could lead to biased findings. Therefore, we propose a method to impute missing disease onset dates under the assumption of missing at random (Little and Rubin, 2002). First, we disaggregate the given surveillance counts to the patient level. For each complete case

Covariable	Parameter	
	μ_l (Standard Error)	σ_l (Standard Error)
Intercept	1.89 (< 0.01)	-0.91 0.013
Gender Male	0.029 (< 0.01)	-0.077 (0.01)
Age Group A35-A59	0.034 (< 0.01)	0.092 (0.014)
Weekend	-0.037 (< 0.01)	-0.07 (0.017)

Table 1: Estimates of linear effects from the imputation model. The reference group are female individuals aged between 15 and 35.

l , the data includes the age/gender group indicator ($x_{l,g}$) and an indicator whether the reporting date was during a weekend ($x_{l,weekend}$). We also have the date of disease onset ($t_{l,o}$) and its reporting ($t_{l,r}$). Following Gönther et al. (2020) and Glöckner et al. (2020) we use the subset of the data without any missing dates to fit a regression model for the time span between onset of disease and its reporting through a positive test, which we define as $d_l = t_{l,r} - t_{l,o}$. As covariates we take $x_l = (x_{l,g}, x_{l,weekend})$. We also include $t_{l,r}$ itself as a covariate to account for changing testing strategies, e.g. during the early spread the test capacities were limited and patients needed to wait longer for a test to be conducted. We assume that d_l is a realisation of random variable D_l , which follows a Negative Binomial model:

$$D_l \mid x_l, t_{l,r} \sim NB\left(\mu_l = \exp\left\{\theta_\mu^\top x_l + f_\mu(t_{l,r})\right\}, \sigma_l = \exp\left\{\theta_\sigma^\top x_l + f_\sigma(t_{l,r})\right\}\right), \quad (1)$$

where $\mathbb{E}(D_l \mid x_l) = \mu_l$ and $\text{Var}(D_l \mid x_l) = \mu_l + \sigma_l^2$ holds. A discrete-valued distribution appears most suitable, since the patient-level data are available on a daily basis, making the reporting delay inherently discrete. As indicated in (1), we model the location and scale parameter of the distribution by separate linear predictors. Therefore the model is in the family of generalised additive models for location, scale and shape (Rigby and Stasinopoulos, 2005). While the categorical covariates x_l are incorporated using dummy variables, we parametrise the trend effect of the reporting date $t_{l,r}$ by penalized splines (see Eilers and Marx, 1996 for details). After having obtained the estimates, we calculate $\hat{\mu}_l$ and $\hat{\sigma}_l$ for the observations with missing disease onset. We can now simulate D_l from (1) to acquire a full data set. This procedure builds a single imputation step, which is repeated K times.

Through the software package `gamlss` we get estimates for the parameters of the imputation model. The results are given in Table 1 and should be interpreted in regards to the mean and dispersion parameter of the time span between disease onset date and reporting date. In Annex A.2, we perform a sensitivity analysis for this procedure and report the smooth estimates. Lastly, we aggregate the data again to the original weekly scale.

3 Model Formulation

3.1 Age- and Gender-Structured Spatio-Temporal Model

To model the number of infections, we apply a negative binomial ‘*observation-driven*’ model for count data (Cox et al., 1981). By doing so, we assume

$$Y_{i,g,t} \mid x_{i,g,t-1}, y_{i,g,t-1}, a_i, b_i \sim NB(\boldsymbol{\mu}_{i,g,t}, \boldsymbol{\sigma}), \forall i \in \{1, \dots, 401\}, g \in \mathcal{G}, \text{ and } t = 2, \dots, T, \quad (2)$$

where $x_{i,g,t} = (t, x_g, x_{i,g,pop}, x_{i,t,gini}, x_{i,t,sp}, x_{i,coord}, x_{i,soc})$ are the joint covariates derived in Section 2 and \mathcal{G} denotes the set of age/gender groups used from the data. Further, let T be the final week of data we use in the analysis. We parametrise the scale parameter $\boldsymbol{\sigma}$ only by an intercept term since we are interested in drawing conclusions about the effect of the covariates on $\boldsymbol{\mu}_{i,g,t}$. We assume in (2) that the random variable $Y_{i,g,t}$ follows a negative binomial distribution conditional on $x_{i,g,t}$ to compensate overdispersion in the observed counts (Ver Hoef and Boveng, 2007). Aligned with models for the spread of infectious diseases, we decompose $\boldsymbol{\mu}_{i,g,t}$ into an endemic and epidemic component:

$$\boldsymbol{\mu}_{i,g,t} = \exp\{\mathbf{v}_{i,g,t}^{END} + \mathbf{v}_{i,g,t}^{EPI}\}, \quad (3)$$

where each part is parametrized as follows:

$$\mathbf{v}_{i,g,t}^{EPI} = \boldsymbol{\theta}_{AR(1)} \log(\tilde{y}_{i,g,t-1} + c) \quad (4)$$

$$\begin{aligned} \mathbf{v}_{i,g,t}^{END} = & \boldsymbol{\theta}_t + \boldsymbol{\theta}_{sex} \mathbb{I}(x_{i,sex} = \text{“Male”}) + \boldsymbol{\theta}_{age} \mathbb{I}(x_{i,age} = \text{“36-59”}) + \boldsymbol{\theta}_{t,gini} x_{i,t-1,gini} \quad (5) \\ & + \boldsymbol{\theta}_{t,sp} x_{i,t-1,sp} + f(x_{i,coord}) + f(x_{i,soc}) + a_i + b_i \mathbb{I}(t = T) + \log(x_{i,g,pop}), \end{aligned}$$

$\tilde{y}_{i,g,t-1} = \frac{10,000 y_{i,g,t-1}}{x_{i,g,pop}}$ in (4) denotes the rate of infections among 10,000 inhabitants in district i in week t . We include a first-order autoregressive term of this rate, since path dependencies and self-exciting behaviour are common with infectious diseases and should therefore be accounted for (Held et al., 2005). In addition, we transform the respective term by $h(x) = \log(x+c)$ to bypass problems with absorbing states of the implied counting process when $\tilde{y}_{i,g,t-1} = 0$ (see Fahrmeir and Tutz, 2001; Fokianos and Tjøstheim, 2011). The value $c \in (0, 1]$ is estimated from the data. More general types of these autoregressive models are proposed by Zeger and Qaqish (1988).

As is evident from (3), we constitute that both the epidemic and endemic components have a multiplicative effect on the observed infection rates. As an alternative, Held et al. (2005) replace the log link by an identity link, although Fokianos and Tjøstheim (2011) and Fokianos et al. (2020) argue for the logarithmic link implied in (3) if additional covariates are available. They further derive theoretical properties, such as ergodicity, in the case of Poisson-distributed target variables under the condition $\boldsymbol{\theta}_{AR(1)} < 1$.

For the endemic part (5), the temporal trend is reflected by piecewise constant fixed effects separately for each week, $\boldsymbol{\theta}_t$. By means of group-specific covariates we control for gender- and age-related effects, $\boldsymbol{\theta}_{sex}$ and $\boldsymbol{\theta}_{age}$ (Walter and McGregor, 2020). The principal covariates, Gini Index and Percentage Staying Put, are modelled by piecewise constants in each week for maximal flexibility. To account for the stylised fact, that the incubation period, i.e., the time between being infected and symptom onset, for COVID-19 is around 5 days (Linton et al., 2020; Li et al., 2020), we lag the information on Gini Index and Percentage Staying Put by one week as indicated in (5).

The bivariate functions $f(x_{i,coord})$ and $f(x_{i,soc})$ display the effects of geographic coordinates and social coordinates on the incidence rate. Details on the type of splines used are given in Section 3.2.

Because super spreader events such as carnival sessions (Streeck et al., 2020) or local outbreaks in major slaughterhouses (Dyal et al., 2020) lead to unobserved heterogeneities, our model comprises two district-specific Gaussian random effects. The random effect a_i governs long-term heterogeneities, while short-term dependencies, i.e., sudden locally confined outbreaks as visible in the last week of Figure 3, are captured by b_i . We assume $a = (a_1, \dots, a_n)^\top \sim N(0, I_n \tau_a^2)$ and $b = (b_1, \dots, b_n)^\top \sim N(0, I_n \tau_b^2)$. The additional parameters τ_a and τ_b are obtained in a data-driven manner using restricted maximum likelihood estimation (Wood, 2011).

Implicitly it is assumed in our model that the entire population is susceptible. This is reasonable when taking into account the current low prevalence of COVID-19 in Germany. Emanating from this observation, the term $\log(x_{i,g,pop})$ is included as an offset in (5). The model is also applicable in later stages of the disease by replacing this offset with the number of susceptible inhabitants in each region.

3.2 Isotropic Smooth Effects

In order to properly incorporate $x_{i,coord}$ and $x_{i,soc}$ in our regression framework, we propose the usage of isotropic splines. These kind of flexible functions were proposed by Duchon (1977) to model multiple covariates by a multivariate term as an alternative to anisotropic tensor products. Isotropic smoothers have the property of giving the identical predictions of the response under arbitrary rotation and reflection of the respective covariates (Wood, 2017). This characteristic is commonly reasonable when working with geographic coordinates $x_{i,coord}$ and in accordance with the uniqueness of the multidimensional scaling results, thus also for $x_{i,soc}$. With respect to the form of the smooth terms, we follow Wood (2003) and use a low-rank approximation of the thin-plate splines introduced in Duchon (1977).

3.3 Estimation and Implementation

We first state how we fix c given one imputation step and then sketch how we account for uncertainty due to multiple imputation when estimating $\hat{\vartheta} = (\hat{\theta}, \hat{\tau}_a, \hat{\tau}_b)$, the vector-valued parameter jointly characterising (3) and the posterior modes of the random effects. Generally, we condition on the observations in $t = 1$, i.e., the week between the 3rd and 9th of March.

In the first step, we define a random grid of $G = 50$ values for $c \in (0, 1]$, denoted by $C = \{c_1, \dots, c_G\}$. Similar to a semiparametric version of Fokianos and Kedem (2004), we construct a penalised likelihood for each district and age/gender group tuple given one imputed dataset generated according to Section 2.3 from (2). The included penalty punishes the roughness of isotropic smooth effects and facilitates the estimation of the random effects in the setting of penalised splines (see Ruppert et al., 2003, 2009 for more details on the duality between penalised splines and mixed models). Combining these separate contributions under independence leads to a joint penalised likelihood, which we denote by $\ell(\theta, \tau_a, \tau_b, c)$. Conditional on c the penalised likelihood is equivalent to a generalised additive mixed model. We then maximise $\ell(\theta, \tau_a, \tau_b | c)$ utilising the comprehensive software package `mgcv` and get $\hat{\theta}_c$, $\hat{\tau}_{a,c}$, and $\hat{\tau}_{b,c}$ (technical details are given in Ruppert et al., 2003 and Wood, 2017). In the consecutive step we evaluate the logarithmic

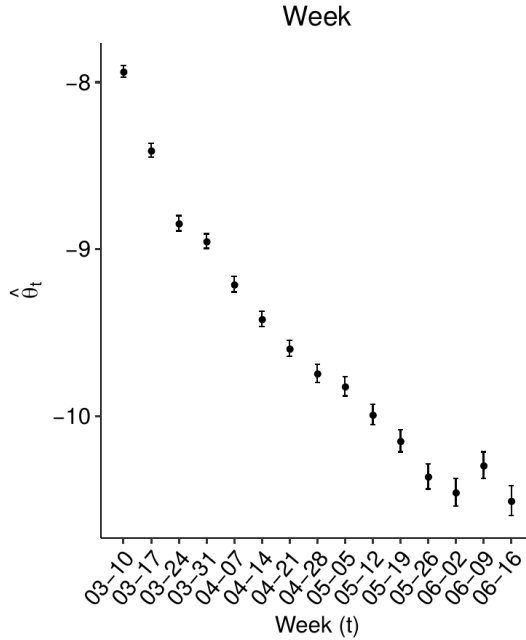


Figure 5: Weekly estimate accompanied by the 95% confidence interval of θ_t .

likelihood at all estimates conditional on $c \in \mathcal{C}$ and fix $\hat{c} = \arg \max_{c \in \mathcal{C}} \ell(\hat{\theta}_c, \hat{\tau}_{a,c}, \hat{\tau}_{b,c} | c)$.

In the second step, we use Rubin's rule to correct for the multiple imputation (Rubin, 1987), since about 30% of the onset dates are being imputed. At first we sample K complete datasets according to Section 2.3. Consecutively, let $\hat{\vartheta}_{(k)} = (\hat{\theta}_{(k)}, \hat{\tau}_{a(k)}, \hat{\tau}_{b(k)})$ be the argument maximising the penalised likelihood given the complete dataset from the k -th imputation step and \hat{c} . Further, we denote by $\hat{V}_{(k)}$ the corresponding variance estimate. In this context, we again make use the software package `mgcv` to obtain $\hat{\vartheta}_{(k)}$ and $\hat{V}_{(k)}$. We can then average the resulting coefficients to obtain $\hat{\vartheta}_{MI} = \frac{1}{K} \sum_{k=1}^K \hat{\vartheta}_{(k)}$ and estimate the variance of $\hat{\vartheta}_{MI}$ through:

$$\widehat{\text{Var}}(\hat{\vartheta}_{MI}) = \bar{V} + (1 + K^{-1})\bar{B},$$

where its components are given by

$$\bar{V} = \frac{1}{K} \sum_{k=1}^K \hat{V}_{(k)}$$

$$\bar{B} = \frac{1}{K-1} \sum_{k=1}^K (\hat{\vartheta}_{(k)} - \hat{\vartheta}_{MI})(\hat{\vartheta}_{(k)} - \hat{\vartheta}_{MI})^\top.$$

In our application, we work with 20 imputations which proved to be sufficient since the estimates between imputation runs varied only marginally.

4 Results

4.1 Trend Effect

To start, the estimate of θ_t is shown in Figure 5. The dynamic of the weekly estimates confirm generally decreasing infection rates over time. Due to the standardisation employed for the principal covariates in the analysis, the temporal trend refers to an average

Covariable	Estimate (Standard Error)	$\exp\{\text{Estimate}\}$ (Standard Error)
Gender Male	-0.071 (0.01)	0.932 (0.009)
Age Group A35-A59	-0.066 (0.01)	0.936 (0.009)
$\log(\tilde{y}_{i,g,t-1} + c)$	0.612 (0.01)	1.845 (0.035)

Table 2: Estimates of linear time-constant effects. The reference group are female individuals aged between 15 and 35. By use of the delta rule we approximated the standard errors of the transformed coefficients in the third row. The value c is set to 0.461.

district where the standardised Gini Index and Percentage Staying Put are zero. For this reason, the standard errors are also extremely narrow.

4.2 Sociodemographic and Epidemic Effects

The linear time-constant estimates are given in Table 2 and exhibit a negative effect for male patients when compared to female patients. For individuals in the second age group, the infection rate is about 7% smaller in comparison to similar people aged between 15 and 34. The coefficient regarding the autocorrelation expresses that one more infection among 10.000 inhabitants in a district during the past week almost doubles the predicted infections for the present week. This dominant finding confirms strong path dependencies in the data.

4.3 Mobility Effects

The time-varying estimates regarding the relative mobility pattern are displayed in Figure 6. Overall, we note a negative influence of the measures proposed in Section 2 on the rate of local COVID-19 infections. In regards to relative importance, both variables rank similarly during the lock-down period persisting until early May. Subsequently, the Gini Index in a region gains weight, while the effect of People Staying Put dissolves. The temporal changes of the respective estimates illustrate a non-linear trend in the estimates, which could not be sufficiently captured by linear effects.

Gini Index: Given all other covariates, Figure 6 (a) suggests that inhabitants with meeting patterns that are centred around a few other districts entail a reduction of infections for a specific district. This tendency is only disrupted in the week starting on March 17th during the early lock-down in Bavaria. The corresponding estimate is positive and significant. Once the national lock-down is ordered, the effect is not significant for one week. The estimated effects remain low but negative until the German government introduces compulsory masks in public areas on April 22nd (Cheng et al., 2020). Thereupon, the effect has a clear downwards tendency. As policymakers slowly lift the lock-down measures, the estimate rises in absolute terms until its maximum in the penultimate week of our observational period. This development may be viewed as evidence that a more focussed attribution of co-location probabilities in a district becomes more crucial over time.

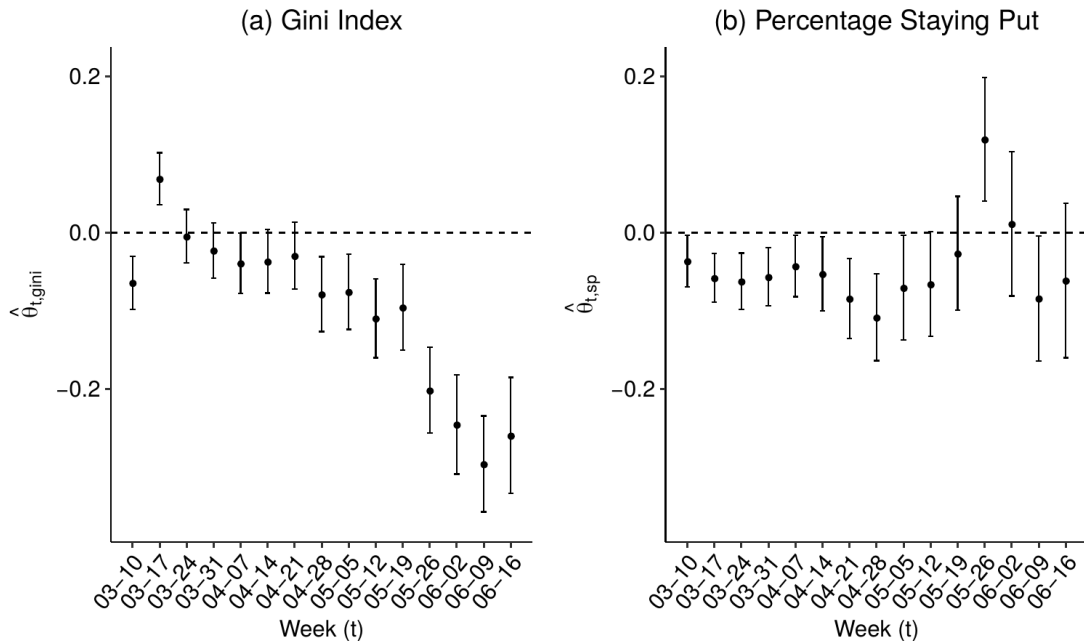


Figure 6: Weekly estimate accompanied by the 95% confidence interval of the Gini Index (a) and the Percentage of People Staying Put (b).

Percentage Staying Put: If the percentage of inhabitants in a district staying put is large in relation to the national tendency, we expect the incidence of infections throughout the lock-down period to be lower. We deduce this result from the largely negative estimates in Figure 6 (b) for the weeks between March 10th and May 18th. Once the orders are relaxed, on the other hand, the influence of the respective covariate largely vanishes. A possible explanation for this phenomenon is that when daily infections decline, most diseases are related to local outbreaks (as already stated in Section 2). These breakouts, in turn, can not be associated with the percentage of people staying put. One exception to this trend is the estimate in the week starting on May 26th, where we encounter a significant positive effect.

4.4 Spatial and Social Connectedness Effects

In our model specification, we incorporate the friendship coordinates and geographic coordinates as two spatial effects. In combination with the two unstructured latent variables, we can disentangle separate influences on the local infection rates of spatial and friendship proximity as well as short- and long-term district-specific deviations from it.

Spatial Effects: Let us start with the smooth spatial effect in Figure 7. Overall, the geographic effects within federal states, delineated by the black borders in Figure 7, are mostly heterogeneous. For instance, the fit for districts in Baden-Württemberg varies between positive, negative, and no effect. On the other hand, an almost uniformly augmented risk of infections is estimated in most parts of Bavaria and Thuringia. Conversely, we remark a negative spatial effect in northern districts of Germany.

We visualise the result of the friendship coordinates in two manners. One may plot the smooth bivariate function in the friendship space, Figure 8 (a), or map the smooth fit on the geographic space, Figure 8 (b). The re-mapping allows for sharp edges in the geographic coordinates. Broadly, the fit differentiates between districts allocated in

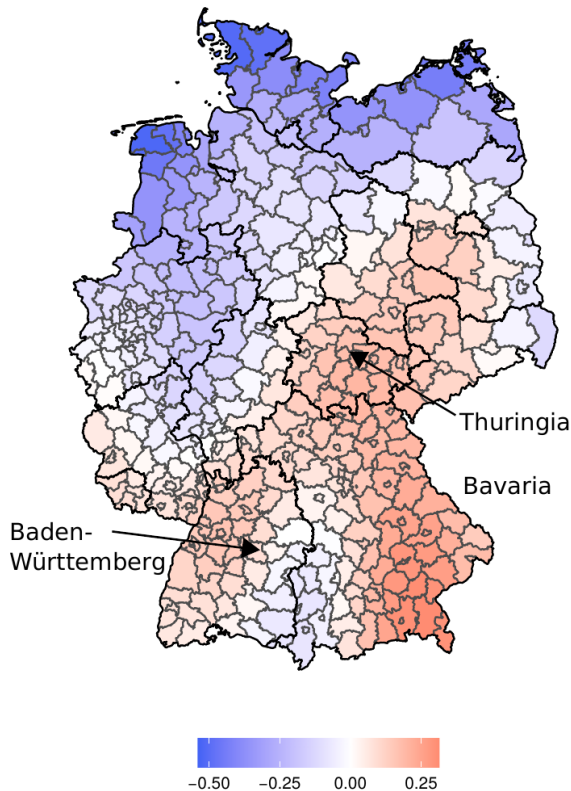


Figure 7: Estimates of the spatial effect $f(x_{i,coord})$ based on geographic coordinates.

former East-Germany (corresponding to MDS coordinates located in the the first quadrant in Figure 8 (a)) and former West-Germany. We observe that the predicted infections are ceteris paribus lower if a district is situated in former East-Germany. Districts allocated in the second and fourth quadrant of Figure 8 (a) (mainly including districts from the states Bavaria, North Rhine-Westphalia and parts of Lower Saxony) are negatively affected by social proximity. Also, Figure 8 (b) demonstrates how the partial effects sometimes change abruptly between large cities and neighbouring districts. For instance, the central position of Berlin is unrelated to the infection rates compared to the negative effect evaluated in Brandenburg. The interplay is reversed in the case of Hamburg when contrasting with surrounding districts in Schleswig Holstein and Lower Saxony.

Unobserved Heterogeneity Effect: In Figure 9 the posterior modes of both random effects evince strong heterogeneities between districts and underpin local differences in the spread of COVID-19. Noticeable estimates of the long-term random effects, Figure 9 (a), reflect early outbreaks in the districts Greiz (Thuringia) and Coesfeld (North Rhine-Westphalia). Some estimates may also be related to heterogeneous testing practices between the districts.

We can trace back most high positive estimates of the short-term random effect to locally confined outbreaks, for instance, Guethersloh and Warendorf (North Rhine-Westphalia). As already stated in Section 2 the proportion of infections attributed to these local events rises as the general level of new cases declines. This finding is supported by the different scales of the two types of random effects and apparent in the estimates $\hat{\tau}_a = 0.235 < \hat{\tau}_b = 0.850$. Therefore, the posterior modes of the short-term effects exhibit higher variances and are larger in absolute terms than the long-term effects.

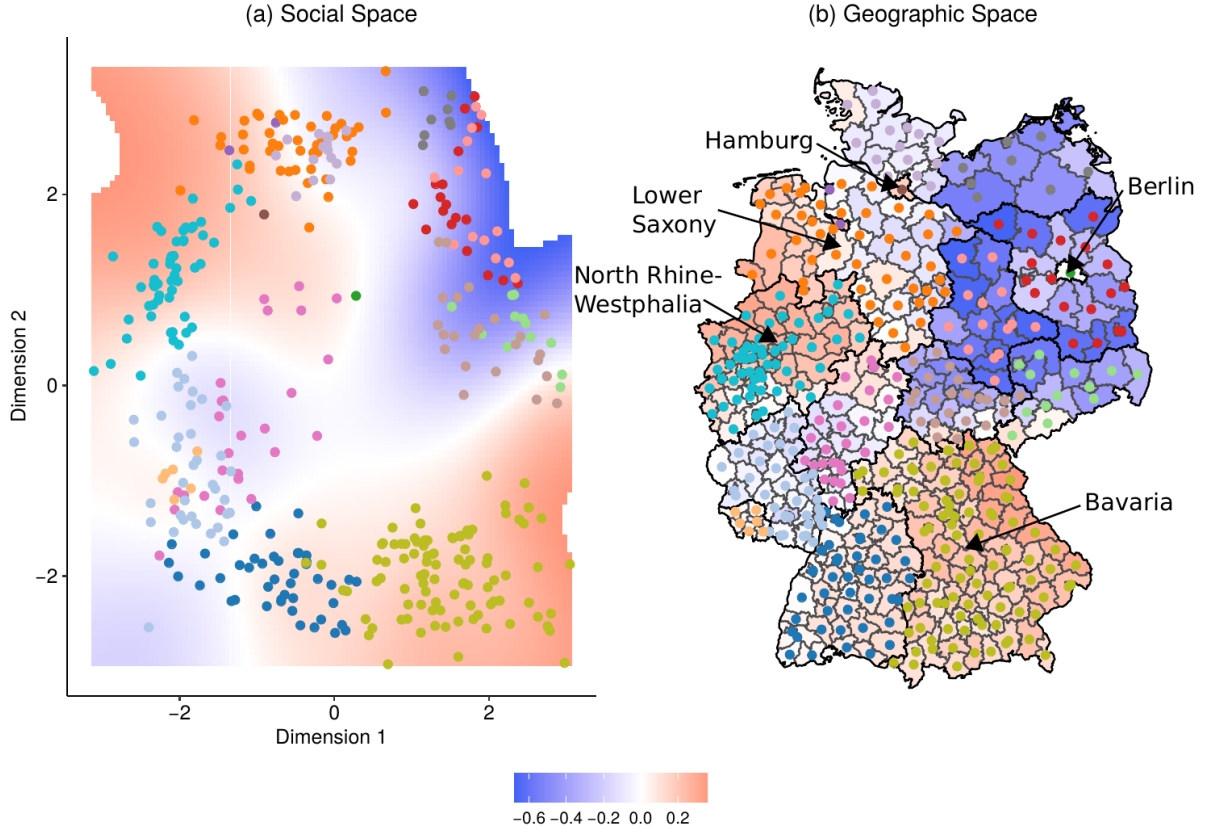


Figure 8: Coordinates of the districts in the friendship distance (a) and transformed to the geographic space (b). The colour in the background represents the partial effects of the corresponding position, $f(x_{i,soc})$. Only the effects in the range of the observations are shown in (a).

Model	Excluded Covariates	$\Delta cAIC$ (Model)
Without Geographic Distance	$f(x_{i,coord})$	4.902
Without Friendship Distance	$f(x_{i,soc})$	7.303
Without Percentage Staying Put	$\theta_{t,sp}$	37.604
Without Gini Index	$\theta_{t,gini}$	281.334
Without Facebook Covariates	$f(x_{i,soc}), \theta_{t,sp}, \theta_{t,gini}$	331.828

Table 3: Alternative Model Specifications and consequential change in corrected AIC value when compared to the full model specified in Section 3.

4.5 Model Assessment

We compare various alternative model specifications to check the robustness of our findings. In particular, we estimate separate models, leaving out one of the spatial terms, the Gini index, the Percentage of People Staying Put, and all Facebook-related covariates. For this endeavour, we utilize the corrected Akaike Information Criterion (cAIC) introduced by Wood et al. (2016) since the effective degrees of freedom need to be adjusted for the additionally estimated variance components if random effects are included (we average the respective values over all imputed datasets). The results in Table 3 support the appropriateness of our final model since the corresponding cAIV value is the lowest. Besides, the change in the cAIC value to the model (2), denoted by $\Delta cAIC$, permits an

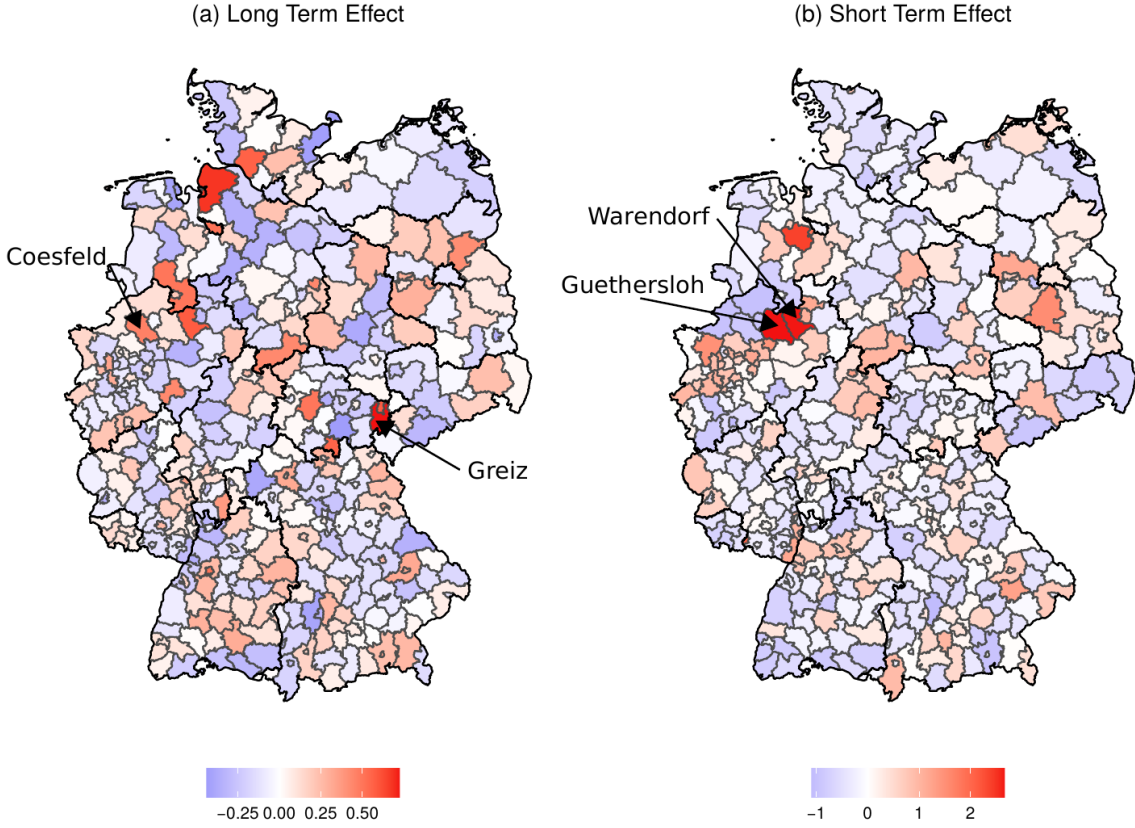


Figure 9: Maximum posterior modes of the long-term (a) and short-term random effects (b).

evaluation of the variable importance of each eliminated covariate. We can conclude from Table 3 that the exclusion of the Gini Index induces the highest loss in cAIC value. Concerning the different types of distances, the friendship distance is more important than the geographic distance.

For further validation, we plot one draw of the randomised quantile residuals in Figure 10 (a). Dunn and Smyth (1996) proposed this type of residual based on the result that evaluating the cumulative distribution function at all observed values of $y_{i,g,t}$ under the estimated parameters should yield uniformly distributed random variables. Transforming these uniform values by the quantile function of the standard normal gives the quantile residuals. To obtain continuous residuals, the values are randomised since the negative binomial distribution in (2) has discrete support. On average, the empirical quantiles are close to the theoretical expectations and do not indicate problems regarding the statistical fit. At the right tail of the distribution, about 25 (out of 24.060) observations exhibit higher deviations from the normal quantiles. The underlying counts are mainly credited to local outbreaks that could not be completely captured by the random effects, namely Coesfeld (Thuringia), Cuxhaven (Lower Saxony), Aichach-Friedberg (Bavaria), Guethersloh, and Warendorf (North Rhine-Westphalia). Additionally, we assess the predictions of the final model through plotting the predicted infections against the observed infections, Figure 10 (b), and a rootogram as proposed by Kleiber and Zeileis (2016), Figure 10 (b). Both visualisations confirm a strong fit of the presented model and proof that the model can sufficiently capture the observed counts of infected individuals.

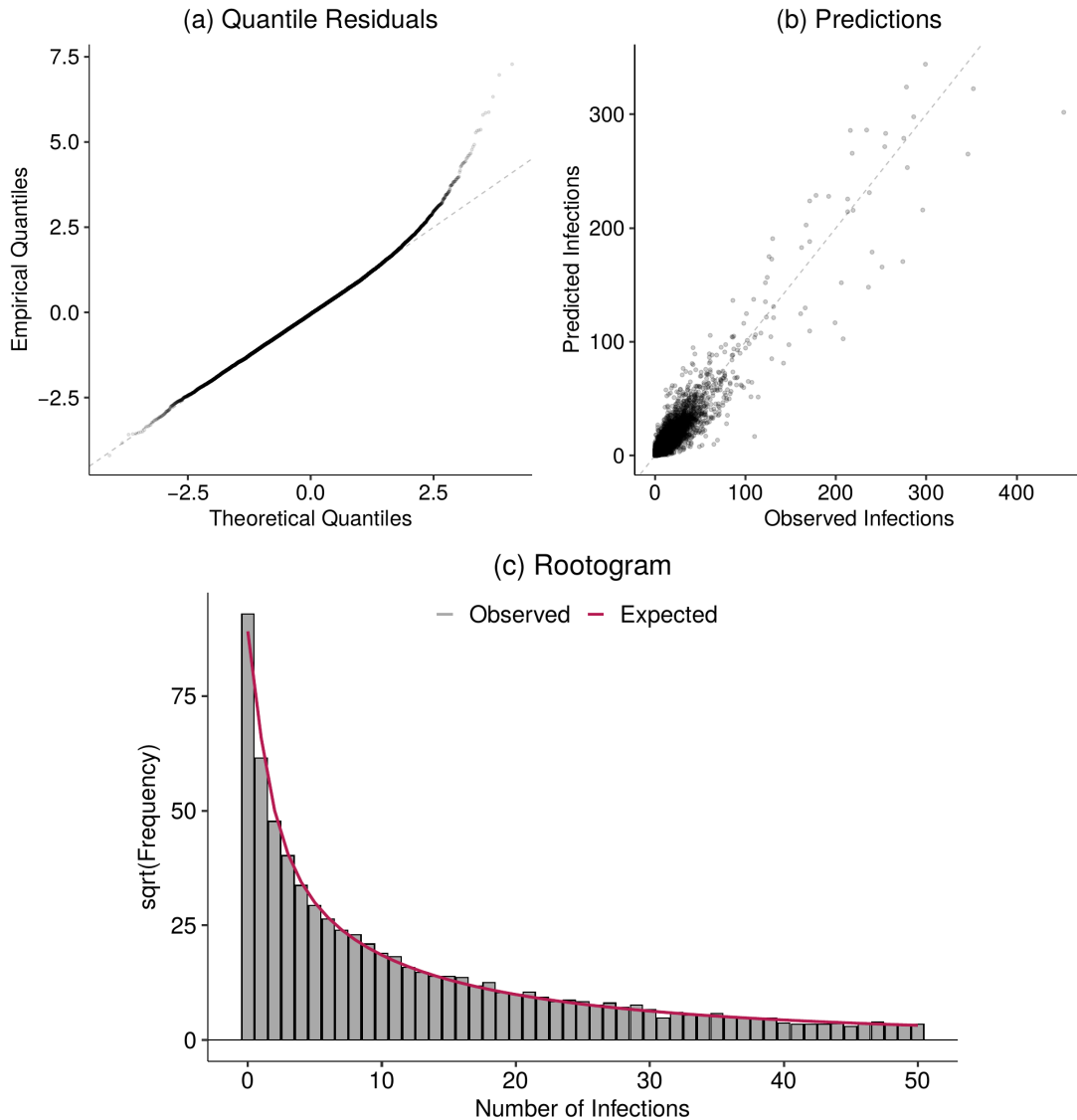


Figure 10: (a): QQ Plot of randomised quantile residuals. (b): Scatter plot of the observed and predicted infection count. (c): Rootogram comparing the observed and expected counts. The grey barplot specifies the observed counts, while the red line gives the expected values under (2).

5 Conclusion

In this writing, our contributions are twofold. Firstly, we used state-of-the-art regression models to quantify the importance of human mobility for understanding the spread of COVID-19 on a local level accounting for their temporal dynamic, latent effects and other covariates. Concerning the relative importance, the concentration of meeting probability attribution proved to be a primary driver of the infection rates. Secondly, we used methods from multivariate statistics to derive friendship coordinates for the federal districts in Germany. Consecutively, we coupled the result with the regression model via isotropic splines and, thereby, revealed a perpetual clustering of communities in former East- and West Germany, which remains existent for COVID-19 infections as the social geographic system proves to be an essential regressor in our application. Moreover, our findings enable a comparative post-hoc evaluation of the district-wise policies undertaken between March

and June 2020. In this respect, the results corroborate the usefulness of interventions limiting trans-district movements and concentrating meeting patterns. Especially, during the last weeks of this study local lock-downs could mitigate the number of infections.

Still, we need to address some limitations of our work, which require additional investigation. The data sources for the infection data include all individuals in Germany that tested positive on COVID-19. Especially during the peak phase in March, these tests were mainly carried out with patients that showed symptoms or had contact with an infected individual. Due to the resulting unknown dark figure of infected persons missing in the public records (Lavezzo et al., 2020), the observed data are a proxy the current epidemiological situation. To control for this possible bias, further research on the prevalence of COVID-19 in Germany and the representability of the official statistics of the real infection occurrence is necessary. Additionally, the research questions posed in this article would greatly benefit from an examination through the lens of analytical sociology (Hedström and Bearman, 2011). This type of analysis, on the other hand, usually necessitates individual-level data, which are at the moment not readily available. Therefore, we can only verify some of the theoretical results of Block et al. (2020) on the macro scale, which does not necessarily translate to the micro scale (Stadtfeld, 2018). Therefore, additional empirical work on the implications of individual behaviour on the spread of COVID-19 is still needed. Nevertheless, our work can give valuable pointers in that regard contingent on the assumption that the mobility patterns of an individual is adequately represented by the corresponding district average.

References

- Asadi, S., N. Bouvier, A. S. Wexler, and W. D. Ristenpart (2020). The coronavirus pandemic and aerosols: Does COVID-19 transmit via expiratory particles? *Aerosol Science and Technology* 54(6), 635–638.
- Bailey, M., R. Cao, T. Kuchler, J. Stroebel, and A. Wong (2018). Social connectedness: Measurement, determinants, and effects.
- Block, P., M. Hoffman, I. J. Raabe, J. Beam Dowd, C. Rahal, R. Kashyap, and M. C. Mills (2020). Social network-based distancing strategies to flatten the COVID-19 curve in a post-lockdown world. *Nature Human Behavior* 4.
- Bonaccorsi, G., F. Pierri, M. Cinelli, A. Flori, A. Galeazzi, F. Porcelli, A. L. Schmidt, C. M. Valensise, A. Scala, W. Quattrocioni, and F. Pammolli (2020). Economic and social consequences of human mobility restrictions under COVID-19. *Proceedings of the National Academy of Sciences* 117(27), 15530–15535.
- Borg, I., P. J. F. Groenen, and P. Mair (2013). *Applied multidimensional scaling*. Springer New York.
- Brandes, U. and C. Pich (2007). Eigensolver methods for progressive multidimensional scaling of large data. In *Graph Drawing 14th International Symposium*, pp. 42–53.
- Brandes, U. and C. Pich (2009). An Experimental Study on Distance-Based Graph Drawing. In *Graph Drawing 16th International Symposium*, pp. 218–229.
- Cailliez, F. (1983). The analytical solution of the additive constant problem. *Psychometrika* 48(2).
- Chan, J. F. W., S. Yuan, K. H. Kok, K. K. W. To, H. Chu, J. Yang, F. Xing, J. Liu, C. C. Y. Yip, R. W. S. Poon, H. W. Tsoi, S. K. F. Lo, K. H. Chan, V. K. M. Poon, W. M. Chan, J. D. Ip, J. P. Cai, V. C. C. Cheng, H. Chen, C. K. M. Hui, and K. Y. Yuen (2020). A familial cluster of pneumonia associated with the 2019 novel coronavirus indicating person-to-person transmission: a study of a family cluster. *The Lancet* 395(10223), 514–523.
- Cheng, C., J. Barceló, A. S. Hartnett, R. Kubinec, and L. Messerschmidt (2020). COVID-19 Government Response Event Dataset (CoronaNet v.1.0). *Nature Human Behaviour*, 1–13.
- Chinazzi, M., J. T. Davis, M. Ajelli, C. Gioannini, M. Litvinova, S. Merler, A. Pastore y Piontti, K. Mu, L. Rossi, K. Sun, C. Viboud, X. Xiong, H. Yu, M. Elizabeth Halloran, I. M. Longini, and A. Vespignani (2020). The effect of travel restrictions on the spread of the 2019 novel coronavirus (COVID-19) outbreak. *Science* 368(6489), 395–400.
- Cho, E., S. A. Myers, and J. Leskovec (2011). Friendship and Mobility: User Movement In Location-Based Social Networks. In *KDD '11: Proceedings of the 17th ACM SIGKDD international conference on Knowledge discovery and data mining*.
- Cox, D. R., G. Gudmundsson, G. Lindgren, L. Bondesson, E. Harsaae, P. Laake, K. Juselius, and S. L. Lauritzen (1981). Statistical Analysis of Time Series: Some Recent Developments. *Scandinavian Journal of Statistics* 8(2), 93–115.

- Cox, M. and T. Cox (2008). Multidimensional Scaling. In C.-h. Chen, W. K. Härdle, and A. Unwin (Eds.), *Handbook of Data Visualization*, pp. 315–347. Springer Berlin Heidelberg.
- Cox, T. and M. Cox (2000). *Multidimensional Scaling*. Chapman & Hall/CRC Boca Raton.
- Duchon, J. (1977). Splines minimizing rotation-invariant semi-norms in Sobolev spaces. In W. Schempp and K. Zeller (Eds.), *Constructive Theory of Functions of Several Variables*, pp. 85–100. Springer Berlin Heidelberg.
- Dunn, P. K. and G. K. Smyth (1996). Randomized Quantile Residuals. *Journal of Computational and Graphical Statistics* 5(3), 236–244.
- Dyal, J. W., M. P. Grant, K. Broadwater, A. Bjork, M. A. Waltenburg, J. D. Gibbins, C. Hale, M. Silver, M. Fischer, J. Steinberg, C. A. Basler, J. R. Jacobs, E. D. Kennedy, S. Tomasi, D. Trout, J. Hornsby-Myers, N. L. Oussayef, L. J. Delaney, K. Patel, V. Shetty, K. E. Kline, B. Schroeder, R. K. Herlihy, J. House, R. Jervis, J. L. Clayton, D. Ortbahn, C. Austin, E. Berl, Z. Moore, B. F. Buss, D. Stover, R. Westergaard, I. Pray, M. DeBolt, A. Person, J. Gabel, T. S. Kittle, P. Hendren, C. Rhea, C. Holsinger, J. Dunn, G. Turabelidze, F. S. Ahmed, S. DeFijter, C. S. Pedati, K. Rattay, E. E. Smith, C. Luna-Pinto, L. A. Cooley, S. Saydah, N. D. Preacely, R. A. Maddox, E. Lundeen, B. Goodwin, S. E. Karpathy, S. Griffing, M. M. Jenkins, G. Lowry, R. D. Schwarz, J. Yoder, G. Peacock, H. T. Walke, D. A. Rose, and M. A. Honein (2020). COVID-19 Among Workers in Meat and Poultry Processing Facilities — 19 States, April 2020. *MMWR. Morbidity and Mortality Weekly Report* 69(18).
- Eilers, P. H. and B. D. Marx (1996). Flexible smoothing with B-splines and penalties. *Statistical Science* 11(2), 89–102.
- Facebook. GeoInsights Help. [https://www.facebook.com/help/geoinsights/880664345608937/?helpref=hc_{_}fnav{&}bc\[0\]=SPAC0HelpCenter{&}bc\[1\]=DiseasePreventionMaps](https://www.facebook.com/help/geoinsights/880664345608937/?helpref=hc_{_}fnav{&}bc[0]=SPAC0HelpCenter{&}bc[1]=DiseasePreventionMaps). Accessed: 2020-06-01.
- Fahrmeir, L. and G. Tutz (2001). *Multivariate Statistical Modelling Based on Generalized Linear Models*. Cham: Springer.
- Flaxman, S., S. Mishra, A. Gandy, H. J. T. Unwin, T. A. Mellan, H. Coupland, C. Whitaker, H. Zhu, T. Berah, J. W. Eaton, M. Monod, Imperial College COVID-19 Response Team, A. C. Ghani, C. A. Donnelly, S. M. Riley, M. A. C. Vollmer, N. M. Ferguson, L. C. Okell, and S. Bhatt (2020). Estimating the effects of non-pharmaceutical interventions on COVID-19 in Europe. *Nature* (OnlineFirst).
- Fokianos, K. and B. Kedem (2004). Partial Likelihood Inference For Time Series Following Generalized Linear Models. *Journal of Time Series Analysis* 25(2), 173–197.
- Fokianos, K., B. StØve, D. TjØstheim, and P. Doukhan (2020). Multivariate count autoregression. *Bernoulli* 26(1), 471–499.
- Fokianos, K. and D. TjØstheim (2011). Log-linear Poisson autoregression. *Journal of Multivariate Analysis* 102(3), 563–578.

- Galeazzi, A., M. Cinelli, G. Bonaccorsi, F. Pierri, A. L. Schmidt, A. Scala, F. Pammolli, and W. Quattrociochi (2020). Human Mobility in Response to COVID-19 in France, Italy and UK.
- Glöckner, S., G. Krause, and M. Höhle (2020). Now-casting the COVID-19 epidemic: The use case of Japan, March 2020. *medRxiv*.
- Guan, W.-j., Z.-y. Ni, Y. Hu, W.-h. Liang, C.-q. Ou, J.-x. He, L. Liu, H. Shan, C.-l. Lei, D. S. Hui, B. Du, L.-j. Li, G. Zeng, K.-Y. Yuen, R.-c. Chen, C.-l. Tang, T. Wang, P.-y. Chen, J. Xiang, S.-y. Li, J.-l. Wang, Z.-j. Liang, Y.-x. Peng, L. Wei, Y. Liu, Y.-h. Hu, P. Peng, J.-m. Wang, J.-y. Liu, Z. Chen, G. Li, Z.-j. Zheng, S.-q. Qiu, J. Luo, C.-j. Ye, S.-y. Zhu, and N.-s. Zhong (2020). Clinical Characteristics of Coronavirus Disease 2019 in China. *New England Journal of Medicine* 382(18), 1708–1720.
- Gönther, F., A. Bender, K. Katz, H. Küchenhoff, and M. Höhle (2020). Nowcasting the covid-19 pandemic in bavaria. *medRxiv*.
- Hedström, P. and P. Bearman (2011). What is Analytical Sociology All About? An Introductory Essay. In P. Bearman and P. Hedström (Eds.), *The Oxford Handbook of Analytical Sociology*. Oxford University Press.
- Held, L., M. Höhle, and M. Hofmann (2005). A statistical framework for the analysis of multivariate infectious disease surveillance counts. *Statistical Modelling* 5(3), 187–199.
- Held, L., S. Meyer, and J. Bracher (2017). Probabilistic forecasting in infectious disease epidemiology: the 13th Armitage lecture. *Statistics in Medicine* 36(22), 3443–3460.
- Held, L. and M. Paul (2012). Modeling seasonality in space-time infectious disease surveillance data. *Biometrical Journal* 54(6), 824–843.
- Holtz, D., M. Zhao, S. G. Benzell, C. Y. Cao, M. Amin Rahimian, J. Yang, J. Allen, A. Collis, A. Moehring, T. Sowrirajan, D. Ghosh, Y. Zhang, P. S. Dhillon, C. Nicolaidis, D. Eckles, and S. Aral (2020). Interdependence and the Cost of Uncoordinated Responses to COVID-19. Technical report.
- Kang, D., H. Choi, J. H. Kim, and J. Choi (2020). Spatial epidemic dynamics of the COVID-19 outbreak in China. *International Journal of Infectious Diseases* 94, 96–102.
- Kissler, S. M., C. Tedijanto, E. Goldstein, Y. H. Grad, and M. Lipsitch (2020). Projecting the transmission dynamics of SARS-CoV-2 through the postpandemic period. *Science* 368(6493), 860–868.
- Kleiber, C. and A. Zeileis (2016). Visualizing Count Data Regressions Using Rootograms. *The American Statistician* 70(3), 296–303.
- Kottasová, I. (2020). Germany reports 650 new coronavirus cases in a meat processing plant - CNN.
- Kraemer, M. U., C. H. Yang, B. Gutierrez, C. H. Wu, B. Klein, D. M. Pigott, L. du Plessis, N. R. Faria, R. Li, W. P. Hanage, J. S. Brownstein, M. Layan, A. Vespignani, H. Tian, C. Dye, O. G. Pybus, and S. V. Scarpino (2020). The effect of human mobility and control measures on the COVID-19 epidemic in China. *Science* 368(6490), 493–497.

- Kuchler, T., D. Russel, and J. Stroebe (2020). The geographic spread of COVID-19 correlates with structure of social networks as measured by Facebook.
- Lavezzo, E., E. Franchin, C. Ciavarella, G. Cuomo-Dannenburg, L. Barzon, C. Del Vecchio, L. Rossi, R. Manganelli, A. Loregian, N. Navarin, D. Abate, M. Sciro, S. Merigliano, E. De Canale, M. C. Vanuzzo, V. Besutti, F. Saluzzo, F. Onelia, M. Pacenti, S. Parisi, G. Carretta, D. Donato, L. Flor, S. Cocchio, G. Masi, A. Sperduti, L. Cattarino, R. Salvador, M. Nicoletti, F. Caldart, G. Castelli, E. Nieddu, B. Labella, L. Fava, M. Drigo, K. A. Gaythorpe, K. E. Ainslie, M. Baguelin, S. Bhatt, A. Boonyasiri, O. Boyd, L. Cattarino, C. Ciavarella, H. L. Coupland, Z. Cucunubá, G. Cuomo-Dannenburg, B. A. Djafaara, C. A. Donnelly, I. Dorigatti, S. L. van Elsland, R. FitzJohn, S. Flaxman, K. A. Gaythorpe, W. D. Green, T. Hallett, A. Hamlet, D. Haw, N. Imai, B. Jeffrey, E. Knock, D. J. Laydon, T. Mellan, S. Mishra, G. Nedjati-Gilani, P. Nouvellet, L. C. Okell, K. V. Parag, S. Riley, H. A. Thompson, H. J. T. Unwin, R. Verity, M. A. Vollmer, P. G. Walker, C. E. Walters, H. Wang, Y. Wang, O. J. Watson, C. Whittaker, L. K. Whittles, X. Xi, N. M. Ferguson, A. R. Brazzale, S. Toppo, M. Trevisan, V. Baldo, C. A. Donnelly, N. M. Ferguson, I. Dorigatti, and A. Crisanti (2020). Suppression of a SARS-CoV-2 outbreak in the Italian municipality of Vo'. *Nature* (OnlineFirst).
- Li, Q., X. Guan, P. Wu, X. Wang, L. Zhou, Y. Tong, R. Ren, K. S. Leung, E. H. Lau, J. Y. Wong, X. Xing, N. Xiang, Y. Wu, C. Li, Q. Chen, D. Li, T. Liu, J. Zhao, M. Liu, W. Tu, C. Chen, L. Jin, R. Yang, Q. Wang, S. Zhou, R. Wang, H. Liu, Y. Luo, Y. Liu, G. Shao, H. Li, Z. Tao, Y. Yang, Z. Deng, B. Liu, Z. Ma, Y. Zhang, G. Shi, T. T. Lam, J. T. Wu, G. F. Gao, B. J. Cowling, B. Yang, G. M. Leung, and Z. Feng (2020). Early Transmission Dynamics in Wuhan, China, of Novel Coronavirus-Infected Pneumonia. *New England Journal of Medicine* 382(13), 1199–1207.
- Li, R., S. Pei, B. Chen, Y. Song, T. Zhang, W. Yang, and J. Shaman (2020). Substantial undocumented infection facilitates the rapid dissemination of novel coronavirus (SARS-CoV2). *Science* 368(6490), 489–493.
- Linton, N. M., T. Kobayashi, Y. Yang, K. Hayashi, A. R. Akhmetzhanov, S.-m. Jung, B. Yuan, R. Kinoshita, and H. Nishiura (2020). Incubation Period and Other Epidemiological Characteristics of 2019 Novel Coronavirus Infections with Right Truncation: A Statistical Analysis of Publicly Available Case Data. *Journal of Clinical Medicine* 9(2), 538.
- Little, R. J. A. and D. B. Rubin (2002). *Statistical Analysis with Missing Data*. Hoboken, NJ, USA: John Wiley & Sons, Inc.
- Lorch, L., W. Trouleau, S. Tsirtsis, A. Szanto, B. Schölkopf, and M. Gomez-Rodriguez (2020). A Spatiotemporal Epidemic Model to Quantify the Effects of Contact Tracing, Testing, and Containment.
- Maas, P., I. Shankar, A. Gros, P. Wonhee, L. McGorman, C. Nayak, and A. P. Dow (2019). Facebook Disaster Maps: Aggregate Insights for Crisis Response & Recovery. *Proceedings of the 16th ISCRAM Conference*.
- Mardia, K. V. (1978). Some properties of classical multi-dimensional scaling. *Communications in Statistics-Theory and Methods* 7(13), 1233–1241.

- Meyer, S. and L. Held (2017). Incorporating social contact data in spatio-temporal models for infectious disease spread. *Biostatistics* 18(2), 338–351.
- Microsoft. Bing Maps Tile System - Bing Maps. <https://docs.microsoft.com/en-us/bingmaps/articles/bing-maps-tile-system>. Accessed: 2020-05-30.
- Oliver, N., B. Lepri, H. Sterly, R. Lambiotte, S. Delataille, M. De Nadai, E. Letouzé, A. A. Salah, R. Benjamins, C. Cattuto, V. Colizza, N. de Cordes, S. P. Fraiberger, T. Koebe, S. Lehmann, J. Murillo, A. Pentland, P. N. Pham, F. Pivetta, J. Saramäki, S. V. Scarpino, M. Tizzoni, S. Verhulst, and P. Vinck (2020). Mobile phone data for informing public health actions across the COVID-19 pandemic life cycle. *Science Advances* 6(23), 1–7.
- Paul, M., L. Held, and A. M. Toschke (2008). Multivariate modelling of infectious disease surveillance data. *Statistics in Medicine* 27(29), 6250–6267.
- Prem, K., Y. Liu, T. W. Russell, A. J. Kucharski, R. M. Eggo, N. Davies, S. Flasche, S. Clifford, C. A. Pearson, J. D. Munday, S. Abbott, H. Gibbs, A. Rosello, B. J. Quilty, T. Jombart, F. Sun, C. Diamond, A. Gimma, K. van Zandvoort, S. Funk, C. I. Jarvis, W. J. Edmunds, N. I. Bosse, J. Hellewell, M. Jit, and P. Klepac (2020). The effect of control strategies to reduce social mixing on outcomes of the COVID-19 epidemic in Wuhan, China: a modelling study. *The Lancet Public Health* 5(5), e261–e270.
- Rigby, R. A. and D. M. Stasinopoulos (2005). Generalized additive models for location, scale and shape. *Journal of the Royal Statistical Society: Series C (Applied Statistics)* 54(3), 507–554.
- Rubin, D. B. (1987). *Multiple Imputation for Nonresponse in Surveys*. New York: Wiley.
- Ruppert, D., M. Wand, and R. J. Carroll (2003). *Semiparametric regression*. Cambridge: Cambridge University Press.
- Ruppert, D., M. Wand, and R. J. Carroll (2009). Semiparametric regression during 2003–2007*. *Electronic Journal of Statistics* 3(3), 1193–1256.
- Stadtfeld, C. (2018). The Micro–Macro Link in Social Networks. *Emerging Trends in the Social and Behavioral Sciences* (OnlineFirst).
- Streeck, H., B. Schulte, B. Kuemmerer, E. Richter, T. Hoeller, C. Fuhrmann, E. Bartok, R. Dolscheid, M. Berger, L. Wessendorf, M. Eschbach-Bludau, A. Kellings, A. Schwaiger, M. Coenen, P. Hoffmann, M. Noethen, A.-M. Eis-Huebinger, M. Exner, R. Schmithausen, M. Schmid, and B. Kuemmerer (2020). Infection fatality rate of SARS-CoV-2 infection in a German community with a super-spreading event. *medRxiv*.
- Van Doremalen, N., T. Bushmaker, D. H. Morris, M. G. Holbrook, A. Gamble, B. N. Williamson, A. Tamin, J. L. Harcourt, N. J. Thornburg, S. I. Gerber, J. O. Lloyd-Smith, E. De Wit, and V. J. Munster (2020). Aerosol and surface stability of SARS-CoV-2 as compared with SARS-CoV-1. *New England Journal of Medicine* 382(16), 1564–1567.
- Ver Hoef, J. M. and P. L. Boveng (2007). Quasi-poisson vs. negative binomial regression: How should we model overdispersed count data? *Ecology* 88(11), 2766–2772.

- Walter, L. A. and A. J. McGregor (2020). Sex-and Gender-specific Observations and Implications for COVID-19. *Western Journal of Emergency Medicine* 21(3), 507–509.
- WHO (2020). Coronavirus disease (COVID-2019) situation reports.
- Wood, S. N. (2003). Thin plate regression splines. Technical Report 1.
- Wood, S. N. (2011). Fast stable restricted maximum likelihood and marginal likelihood estimation of semiparametric generalized linear models. *Journal of the Royal Statistical Society: Series B (Statistical Methodology)* 73(1), 3–36.
- Wood, S. N. (2017). *Generalized additive models: An introduction with R*. Boca Raton: CRC press.
- Wood, S. N., N. Pya, and B. Säfken (2016). Smoothing parameter and model selection for general smooth models. *Journal of the American Statistical Association* 111(516), 1548–1563.
- Wu, Y.-C., C.-S. Chen, and Y.-J. Chan (2020). The outbreak of COVID-19. *Journal of the Chinese Medical Association* 83(3), 217–220.
- Young, G. and A. S. Householder (1938). Discussion of a set of points in terms of their mutual distances. *Psychometrika* 3(1), 19–22.
- Zeger, S. L. and B. Qaqish (1988). Markov Regression Models for Time Series: A Quasi-Likelihood Approach. *Biometrics* 44(4), 1019–1031.

Acknowledgement

The project was supported by the European Cooperation in Science and Technology [COST Action CA15109 (COSTNET)]. This work has been funded by the German Federal Ministry of Education and Research (BMBF) under Grant No. 01IS18036A. The authors of this work take full responsibility for its content.

A Annex

A.1 Multidimensional Scaling

In order to determine the information given in the pairwise social connectedness indices $x_{soc} = (x_{ij,soc})_{i,j=1,\dots,n}$ for explaining the spread of COVID-19 in Germany, we use techniques from multivariate statistics (Cox and Cox, 2000). Thereby, we can derive a low-dimensional representation of the network on the actor level and guarantee interpretable as well as transparent results. More specifically, we apply metric multidimensional scaling (MDS) to represent dissimilarity matrices in a lower-dimensional geometric space that preserves the dissimilarities through euclidean distances (Borg et al., 2013). Related methods are also used as a visualisation tool to draw networks (see Brandes and Pich, 2007, 2009). To illustrate the application of this algorithm, one can think of MDS as a technique to reverse engineer geographic coordinates that are unique up to scale and rotation from distances between cities (Young and Householder, 1938).

At first, we transform the similarities expressed by the counts of friendship ties between the districts x_{soc} to dissimilarities. In our application, the measure of dissimilarity is given by $d_{soc} = (\frac{1}{x_{ij,soc}})_{i \neq j=1,\dots,n}$ and $d_{ii,soc} = 0$. Since the dissimilarity matrix is symmetric and non-negative, but there is no general guarantee that the entries of d_{soc} are euclidean, we add the constant c to the off-diagonal elements to ensure that the distances between the found coordinates are euclidean (Cailliez, 1983; Mardia, 1978). In order to derive these p -dimensional coordinates $x_{i,soc} = (x_{i,1}, \dots, x_{i,p}) \forall i = 1, \dots, n$ from the dissimilarity matrix d_{soc} , the objective is to minimise the squared error between the entries of d_{soc} and the euclidean distances calculated with the respective coordinates:

$$(x_{1,soc}^\top, \dots, x_{n,soc}^\top) = \underset{\tilde{x} \in \mathbb{R}^{p \times n}}{\operatorname{argmin}} \left(\sum_{i \neq j} (d_{ij,soc} + c - \|\tilde{x}_{i,soc} - \tilde{x}_{j,soc}\|^2) \right)^{1/2}, \quad (6)$$

in our case we set $p = 2$. See Cox and Cox (2000); Borg et al. (2013) for methods to find x such that (6) holds. Since the resulting coordinates, represented by $x_{i,soc} \forall i \in \{1, \dots, n\}$, can only be determined up to the location, rotation, and reflection, we additionally use Procrustes Analysis (Cox and Cox, 2008) to use the rotation most similar to the geographic coordinates in Figure 8 and the subsequent analysis. This does not change the estimates or inference, since we apply isotropic smooth terms (further details are given in Section 3.2).

A.2 Further Results from the Disease Onset Imputation

First, we give the smooth estimates of the temporal trends in the model for the time span between the disease onset and the reporting date. Consecutively, we carry out a sensitivity analysis of the imputation procedure introduced in Section 2.3.

A.2.1 Smooth Estimate

In Figure 11, we observe a negative temporal trend for reporting dates during the beginning of March. But once we see more reported cases in April, the mean time span lengthens. During this period also the σ parameter is higher, leading to a higher variance of the respective observations. After May, the average delay decreases but increases again during the last week of this study.

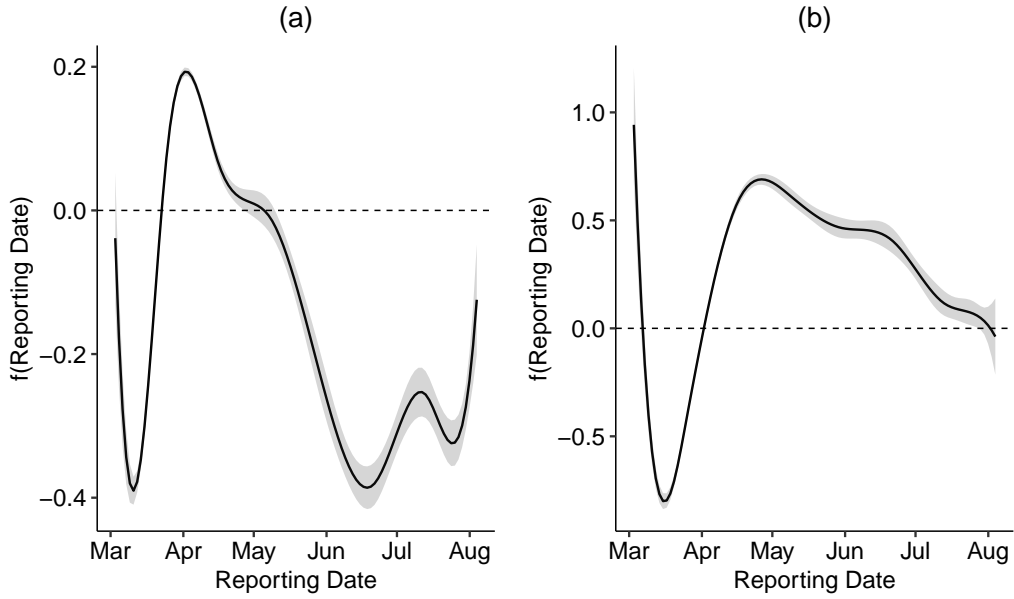


Figure 11: Smooth temporal trends of the μ (a) and σ (b) parameter of the disease onset model.

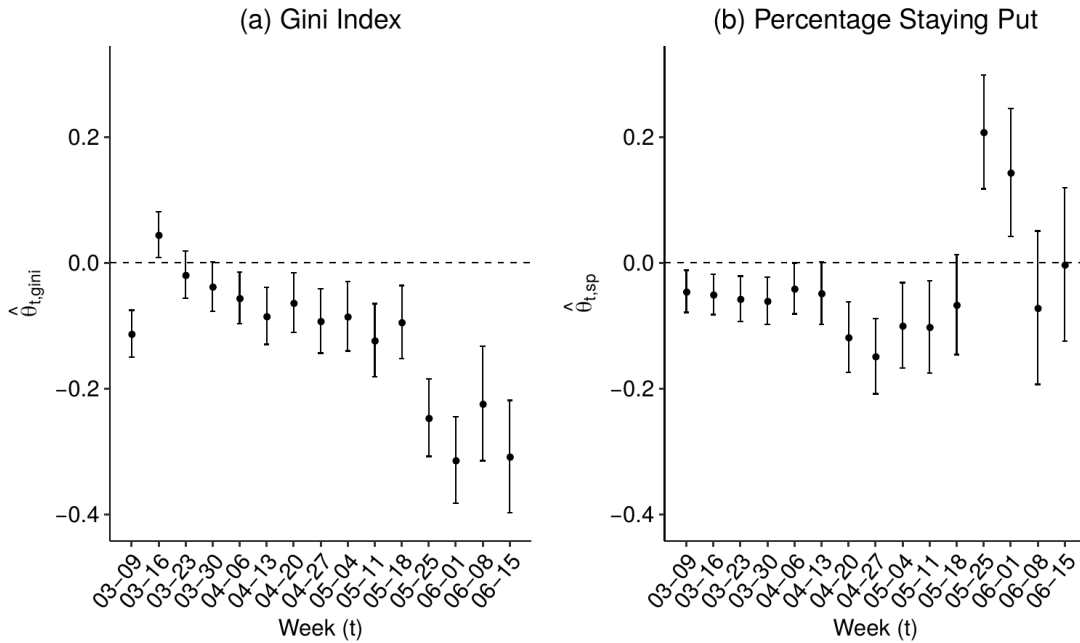


Figure 12: Weekly estimate accompanied by the 95% confidence interval of the Gini Index (a) and the Percentage of People Staying Put (b) when excluding all cases where the disease onset date is missing.

A.2.2 Sensitivity Check of Disease Onset Imputation

In Figure 12 - 15, the results of the model are given if we only include the cases with an observed date of disease onset. The fundamental findings of Section 4 are robust to the imputation method used.

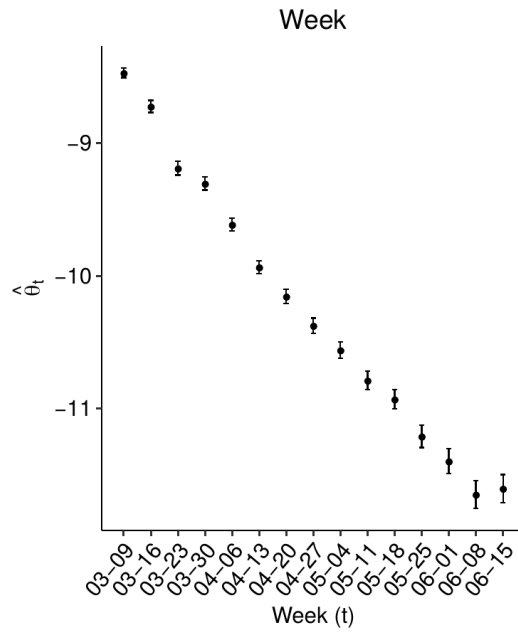


Figure 13: Weekly estimate accompanied by the 95% confidence interval of θ_t when excluding all cases where the disease onset date is missing.

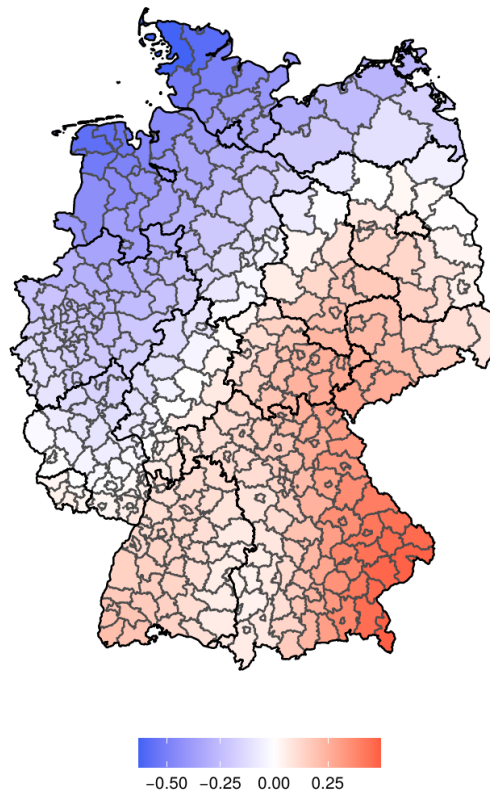


Figure 14: Estimates of the spatial effect $f(x_{i,coord})$ when excluding all cases where the disease onset date is missing.

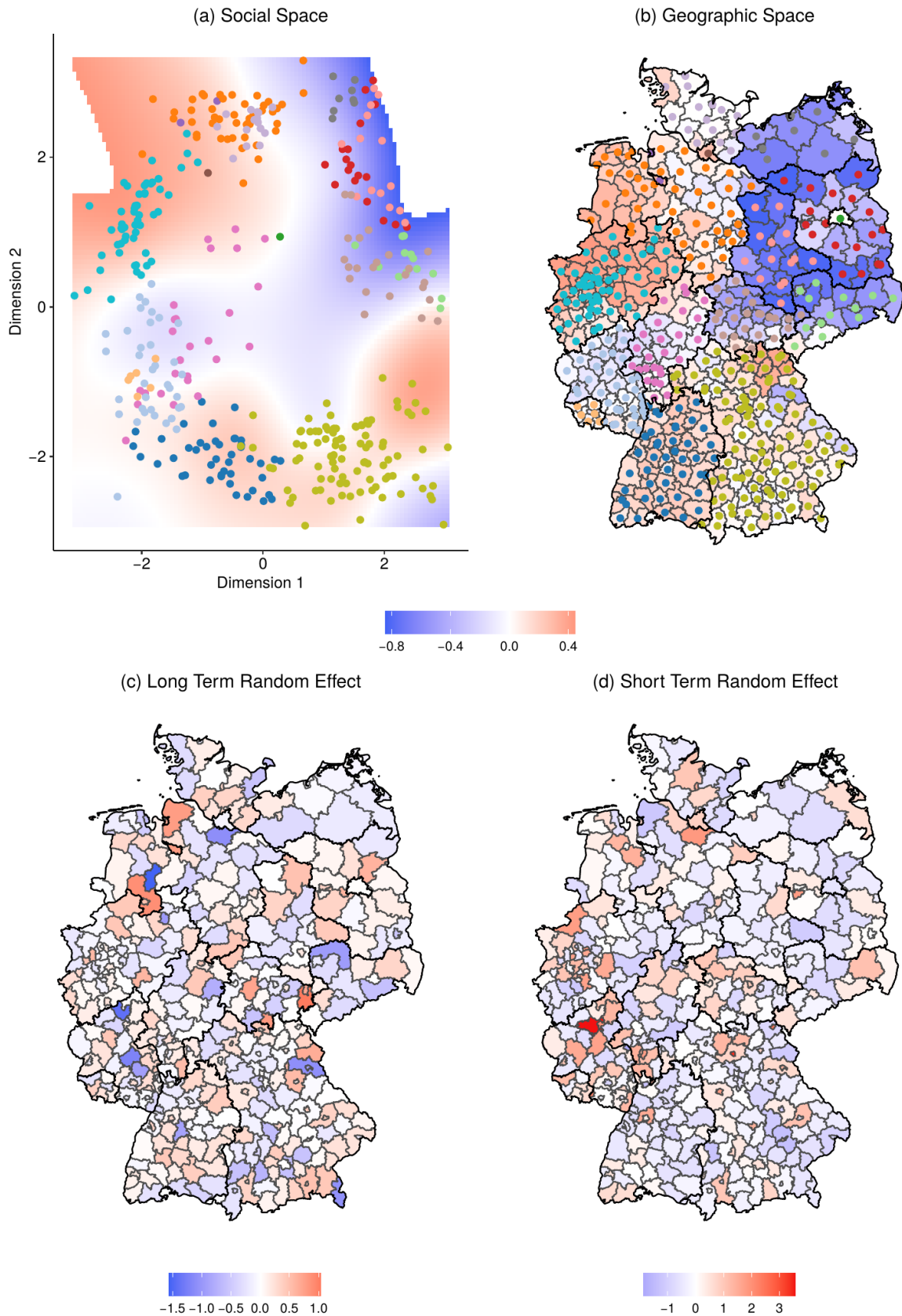


Figure 15: Coordinates of the districts in the friendship distance (a) and transferred to the geographic (b) space. The colour in the background represents the estimates of the smooth fit $f(x_{i,soc})$ when excluding all cases where the disease onset date is missing. The maximum posterior modes of the long-term (c) and short-term random effects (d) are given as well.